METHODS FOR EVALUATING RHEOLOGICAL COEFFICIENTS OF SELF-COMPACTING CONCRETE BY NUMERICAL ANALYSIS

(Translation from Proceedings of JSCE, No.648/V-47, May 2000)

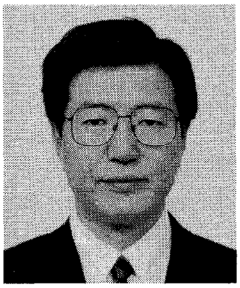

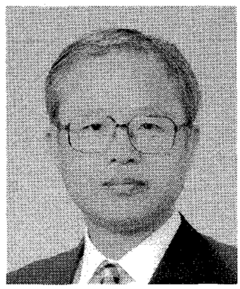

Takeshi KOKADO Takashi HOSODA Toyoaki MIYAGAWA

The validity and limitations of numerical analysis for the simulation of the flow behavior of self-compacting concrete in slump flow tests are discussed by comparing results with experimental values in the case of high-flow mortar. It is found that, when the self-compacting concrete has a high deformation rate, it is necessary to model the effect of the slump cone sidewalls as the cone is raised. Further, it is determined that when the ratio of plastic viscosity to yield value is 1.0 s or more, the relationship between flow radius and time taken to reach the flow radius is accurately simulated by numerical analysis (±20%). The effects of yield value and plastic viscosity on the time taken to reach flow radiuses of 200 mm and 250 mm are clarified, and methods of evaluating the rheological coefficients of self-compacting concrete using the slump flow test are proposed.

Key Words: *self-compacting concrete, slump flow, Bingham plastics, rheological coefficients, yield value, plastic viscosity, numerical analysis, MAC method*

Takeshi KOKADO is a manager in the Construction Materials Development Div. of Nippon Steel Corporation. He received his Doctor of Engineering Degree from Kyoto University in 1999. His research interests relate to the rheology of fresh concrete and the application of self-compacting concrete to steel-concrete composite structures. He is a member of the RILEM, JCI, and JSCE.

Takashi HOSODA is an Associate Professor in the Department of Civil Engineering at Kyoto University. He received his Doctor of Engineering Degree from Kyoto University in 1990. He is the author of a number of papers dealing with open channel hydraulics, turbulent flows, and river channel processes. He is a member of the IAHR, JSFM, JSCFD, and JSCE.

Toyoaki MIYAGAWA is a Professor in the Department of Civil Engineering at Kyoto University. He received his Doctor of Engineering Degree from Kyoto University in 1985. He is the author of a number of papers dealing with the durability, maintenance, and repair of reinforced concrete structures. He is a member of the ACI, RILEM, fib, JSMS, JCI, and JSCE.

1. Introduction

When using self-compacting concrete[1], [2], it is important to determine whether or not it will fill every nook and cranny of the form. This entails rationalizing the processes of material selection, mix design, and quality control and then developing methods of evaluating the filling characteristics of self-compacting concrete. In pursuing this objective, it is necessary to understand the flow and deformation characteristics — or rheological properties — of self-compacting concrete and also to quantitatively determine the relationships between evaluation indexes such as the slump flow and the time taken to reach a particular radius (referred to here as the flow time) and the various rheological coefficients of self-compacting concrete.

The authors have in the past theoretically discussed the relationship between slump flow and yield value by considering the basic flow equations, and have derived theoretical equations to describe the relationship between the slump flow and yield value of Bingham fluids. Using sphere drag tests and slump flow tests on high-flow mortar, they have also confirmed that the yield value as determined by a sphere drag test agrees well with that calculated from the slump flow[3].

The authors have, furthermore, clarified that there is good correlation between flow time and plastic viscosity; this was also determined from sphere drag tests and slump flow tests[4]. That is, the time taken to reach a flow radius of 200 mm correlates well with plastic viscosity η_{pl} when the slump flow is above 500 mm, and the time taken to reach a flow radius of 250 mm correlates well with plastic viscosity η_{pl} when the slump flow exceeds 600 mm. There were, however, some deviations in the correlations between flow time and plastic viscosity in these tests. This is presumably because flow time is affected not only by the plastic viscosity but also by the yield value.

This new study clarifies the validity of simulating the flow behavior of self-compacting concrete in slump flow tests by numerical fluid analysis and its limitations. It results in a quantitative relationship between the rheological coefficients and the flow time of self-compacting concrete.

2. Basic Equations

2.1 Constitutive Equations

The constitutive equation for an incompressible viscous fluid is given as Eq. (1).

$$\tau'_{ij} = 2\eta e_{ij} \tag{1}$$

where, τ'_{ij} is the stress-deviation tensor; η is viscosity; and e_{ij} is the strain rate tensor.

In sphere drag tests with high-flow mortar, there is a linear relationship between pull-up rate v and drag force F for a steel sphere of diameter $D = 31.75$ mm when the pull-up rate ranges from 10 to 60 mm/s. This relationship is valid down to a pull-up rate of 2 mm/s, depending on the yield value τ_y and the plastic viscosity η_{pl}. This confirms that high-flow mortar can be treated as a Bingham fluid[4].

The constitutive equation for a Bingham fluid can be expressed as in Eq. (2), which incorporates the extension by Hohenemser and Prager into any arbitrary stress state[5].

$$2\eta_{pl} e_{ij} = \begin{cases} 0 & \left(\sqrt{J'_2} \le \tau_y\right) \\ \left(1 - \dfrac{\tau_y}{\sqrt{J'_2}}\right)\tau'_{ij} & \left(\sqrt{J'_2} > \tau_y\right) \end{cases} \tag{2}$$

where, η_{pl} is plastic viscosity; τ_y is yield value; and

J'_2 $\left(= \frac{1}{2}\left(\tau'^2_{rr} + \tau'^2_{\theta\theta} + \tau'^2_{zz}\right) + \tau'^2_{r\theta} + \tau'^2_{\theta z} + \tau'^2_{zr}\right)$ is the second invariant of the stress-deviation tensor.

In incompressible viscous fluids, including Bingham fluids, the second invariant of the strain tensor I_2 is given by Eq. (3), and the relationship given by Eq. (4) holds between J'_2 and I_2.

$$I_2 = \frac{1}{2}\left(e_{rr}^2 + e_{\theta\theta}^2 + e_{zz}^2\right) + e_{r\theta}^2 + e_{\theta z}^2 + e_{zr}^2 \tag{3}$$

$$J'_2 = 4\eta^2 I_2 \tag{4}$$

When $\sqrt{J'_2} > \tau_y$ in the Bingham fluid, Eq. (2) indicates us that the stress-deviation tensor τ'_{ij} can be written

$$\tau'_{ij} = 2\eta_{pl} \frac{\sqrt{J'_2}}{\sqrt{J'_2} - \tau_y} e_{ij} \tag{5}$$

Then, from Eqs. (4) and (5), the second invariant of the stress-deviation tensor J'_2 is given by

$$J'_2 = 4\left(\eta_{pl} \frac{\sqrt{J'_2}}{\sqrt{J'_2} - \tau_y} \right)^2 I_2 \tag{6}$$

For $\sqrt{J'_2} > \tau_y$, the relationship between $\sqrt{J'_2}$ and $\sqrt{I_2}$ is given by

$$\sqrt{J'_2} = 2\eta_{pl}\sqrt{I_2} + \tau_y \qquad \left(\sqrt{J'_2} > \tau_y\right) \tag{7}$$

Transforming Eq. (5),

$$\tau'_{ij} = 2\eta_{pl} \frac{\sqrt{J'_2} - \tau_y + \tau_y}{\sqrt{J'_2} - \tau_y} e_{ij} = 2\left(\eta_{pl} + \frac{\tau_y}{2\dfrac{\sqrt{J'_2} - \tau_y}{2\eta_{pl}}} \right) e_{ij} \tag{8}$$

Since Eq. (7) can be rewritten as

$$\sqrt{I_2} = \frac{\sqrt{J'_2} - \tau_y}{2\eta_{pl}} \tag{9}$$

substitution into Eq. (8) then yields:

$$\tau'_{ij} = 2\left(\eta_{pl} + \frac{\tau_y}{2\sqrt{I_2}} \right) e_{ij} \tag{10}$$

For $\sqrt{J'_2} \leq \tau_y$, the stress-deviation tensor cannot be identified, which is problematic from a numerical analysis perspective. To overcome this, it is assumed that when the square root $\sqrt{I_2}$ of the second invariant of the strain rate tensor is equal to or less than a critical value, $\sqrt{I_{2_c}}$, the relationship between $\sqrt{I_2}$ and $\sqrt{J'_2}$ is represented by a straight line that passes through the origin and intersects Eq. (7) at $\sqrt{I_{2_c}}$ (refer to **Fig. 1**).

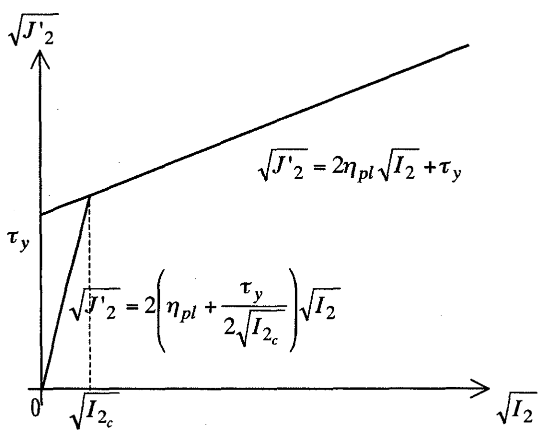

Fig. 1 Relationship between $\sqrt{I_2}$ and $\sqrt{J'_2}$

$$\sqrt{J'_2} = 2\left(\eta_{pl} + \frac{\tau_y}{2\sqrt{I_{2_c}}}\right)\sqrt{I_2} \qquad \left(\sqrt{I_2} \le \sqrt{I_{2_c}}\right) \tag{11}$$

When $\sqrt{I_2} < \sqrt{I_{2_c}}$, the stress-deviation tensor τ'_{ij} is given by

$$\tau'_{ij} = 2\left(\eta_{pl} + \frac{\tau_y}{2\sqrt{I_{2_c}}}\right)e_{ij} \tag{12}$$

From Eqs. (10) and (12), the constitutive equation of the Bingham fluid as defined for use in the numerical analysis is expressed as follows:

$$\tau_{ij} = -p\delta_{ij} + 2\eta e_{ij} \tag{13}$$

where, τ_{ij} is the stress tensor; p is pressure; δ_{ij} is the Kronecker delta; and η is viscosity.

The viscosity η is given by

$$\eta = \eta_{pl} + \frac{\tau_y}{2\sqrt{I_2}} \qquad \left(\sqrt{I_2} > \sqrt{I_{2_c}}\right) \tag{14}$$

$$\eta = \eta_{pl} + \frac{\tau_y}{2\sqrt{I_{2_c}}} \qquad \left(\sqrt{I_2} \le \sqrt{I_{2_c}}\right) \tag{15}$$

2.2 Basic Equations of Flow

The motion of a fluid is generally represented in terms of the equation of continuity and the equations of motion. In applying numerical analysis to the problem of concrete slump flow, the problem can be handled as an axisymmetric flow originating at the center of the slump cone and parabolically spreading. Fresh concrete can be regarded as an incompressible fluid.

Using the cylindrical coordinate system (r, θ, z) with the z- and r-axes taken to be in the axial and radial directions of the slump cone, respectively, the equations of continuity and motion can be represented as follows:

Equation of continuity

$$\frac{1}{r}\frac{\partial}{\partial r}(rv_r) + \frac{\partial v_z}{\partial z} = 0 \tag{16}$$

Equations of motion

$$\frac{\partial v_r}{\partial t} + \frac{1}{r}\frac{\partial (rv_r^2)}{\partial r} + \frac{\partial (v_r v_z)}{\partial z} = \frac{1}{\rho}\left(\frac{\partial \tau_{rr}}{\partial r} + \frac{\tau_{rr} - \tau_{\theta\theta}}{r} + \frac{\partial \tau_{zr}}{\partial z}\right) \tag{17}$$

$$\frac{\partial v_z}{\partial t} + \frac{1}{r}\frac{\partial (rv_r v_z)}{\partial r} + \frac{\partial v_z^2}{\partial z} = \frac{1}{\rho}\left(\frac{\partial \tau_{rz}}{\partial r} + \frac{\tau_{rz}}{r} + \frac{\partial \tau_{zz}}{\partial z}\right) - g \tag{18}$$

where, v_i is velocity component in the i-direction; ρ is density; g is the acceleration due to gravity; and t is time.

Using Eq. (13), these equations of motion can be rewritten as below.

$$\frac{\partial v_r}{\partial t} + \frac{1}{r}\frac{\partial (rv_r^2)}{\partial r} + \frac{\partial (v_r v_z)}{\partial z} = -\frac{1}{\rho}\frac{\partial p}{\partial r} + \frac{2\eta}{\rho}\frac{\partial^2 v_r}{\partial r^2} + \frac{2\eta}{\rho r}\left(\frac{\partial v_r}{\partial r} - \frac{v_r}{r}\right) + \frac{\eta}{\rho}\frac{\partial^2 v_r}{\partial z^2} + \frac{\eta}{\rho}\frac{\partial^2 v_z}{\partial r \partial z} \tag{19}$$

$$\frac{\partial v_z}{\partial t} + \frac{1}{r}\frac{\partial (rv_r v_z)}{\partial r} + \frac{\partial v_z^2}{\partial z} = -\frac{1}{\rho}\frac{\partial p}{\partial z} + \frac{\eta}{\rho}\frac{\partial^2 v_r}{\partial r \partial z} + \frac{\eta}{\rho}\frac{\partial^2 v_z}{\partial r^2} + \frac{\eta}{\rho r}\frac{\partial v_r}{\partial z} + \frac{\eta}{\rho r}\frac{\partial v_z}{\partial r} + \frac{2\eta}{\rho}\frac{\partial^2 v_z}{\partial z^2} - g \tag{20}$$

2.3 Equation of Pressure

When calculating flow for a fluid with a free surface using numerical analysis, it is necessary to determine the pressure field for the entire computational region. The pressure field can be obtained by numerically calculating the equation of pressure (21) for the pressure P as derived from the equations of motion, Eqs. (19) and (20)[6].

$$\frac{1}{\rho}\left\{\frac{1}{r}\frac{\partial}{\partial r}\left(r\frac{\partial p}{\partial r}\right)+\frac{\partial^2 p}{\partial z^2}\right\}=-2\left\{\left(\frac{\partial v_r}{\partial r}\right)^2+\left(\frac{\partial v_r}{\partial r}\right)\left(\frac{\partial v_z}{\partial z}\right)+\left(\frac{\partial v_z}{\partial r}\right)\left(\frac{\partial v_r}{\partial z}\right)+\left(\frac{\partial v_z}{\partial z}\right)^2\right\}-\frac{\partial D}{\partial t}+\frac{\eta}{\rho}\nabla^2 D \quad (21)$$

where,

$$D=\frac{1}{r}\frac{\partial}{\partial r}(rv_r)+\frac{\partial v_z}{\partial z} \quad (22)$$

$$\nabla^2 D=\frac{1}{r}\frac{\partial}{\partial r}\left(r\frac{\partial D}{\partial r}\right)+\frac{\partial^2 D}{\partial z^2} \quad (23)$$

3. Numerical Analysis

3.1 Numerical Analysis Method

The flow of concrete in a slump flow test is a free-surface flow, so the Marker and Cell method (MAC method) developed by Harlow and Welch for free-surface flows is used[7].
The grid system consists of a staggered mesh, in which the pressure is defined at the center of each cell and the velocity component is defined at the boundary between cells.
The equation of continuity (16), equations of motion (19) and (20), and the equation of pressure (21) are discretized using Harlow and Welch's method[7]. The convective terms in the equations of motion (the second term on the left-hand side of Eq. (19) and the third term on the left-hand side of Eq. (20)) are discretized by the first-order upwind difference scheme.
To determine a suitable cell size, numerical analysis was carried out in advance for two cases: one in which the cell size was set at $\Delta r = 5$ mm in the r-direction (radial direction) and $\Delta z = 5$ mm in the z-direction (height direction); and a second in which Δr and Δz were each set at 2.5 mm. Little or no difference was noted in the results obtained in the two cases. The cell size is thus set at $\Delta r = \Delta z = 5$ mm. The computational region is assumed to measure $100\Delta r$ in the r-direction and $64\Delta z$ in the z-direction.

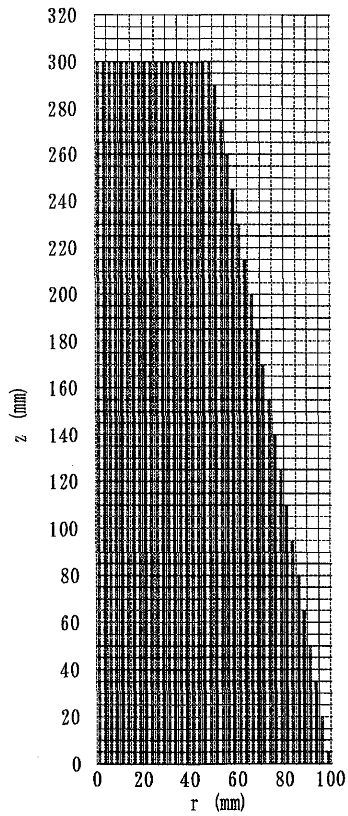

Fig. 2 Arrangement of marker particles at start of computation

3.2 Initial Conditions

The slump cone remains filled with concrete until it is raised. Marker particles with a particular initial arrangement in the cells within the slump cone are used to track changes with time as the slump cone is pulled up. When computation begins (t = 0), the arrangement of the marker particles is as shown in **Fig. 2**. That is, where $0 < r \leq 50$ mm, there are $4 \times 2 = 8$ marker particles per cell, while for $50\text{mm} < r \leq 100\text{mm}$, there are 4 particles per surface cell. 7,160 marker particles are used in total.

3.3 Boundary Conditions

Non-slip condition at the bottom surface and free slip along the axis of symmetry are used as the boundary conditions.

3.4 Modeling of Slump Cone Sidewall

There have been various studies[8],[9], [10], [11] of the deformation behavior of concrete during slump tests using numerical analysis. Since most of these studies address ordinary concrete whose consistency can be indicated by slump, however, the slump cone is assumed to have disappeared instantaneously once computation starts.

This study, however, addresses self-compacting concrete that has a lower consistency. In this case, it is considered necessary to model the effect of the slump cone sidewall as the cone is raised. In experiments by the authors, the slump cone is raised at a rate of about 40 mm/s. The sidewall is approximated by a cylinder with a radius of 100 mm by placing a vertical barrier at r = 100 mm. This boundary wall is set up to rise in 0.125 s per cell (or 5 mm ÷ 40 mm/s). The boundary conditions for the wall surface is that there is no slip, as is the case with the bottom surface.

3.5 Numerical Stability Condition

The convective terms in the equations of motion, Eqs. (19) and (20), are discretized using the first-order upwind scheme. Equation (24) is applied to the differential stability condition[12].

$$\Delta t \leq \frac{1}{2\frac{\eta}{\rho}\left(\frac{1}{\Delta r^2}+\frac{1}{\Delta z^2}\right)+\frac{|v_r|}{\Delta r}+\frac{|v_z|}{\Delta z}} \tag{24}$$

3.6 Physical Quantities

The rheological coefficients (yield value τ_y and plastic viscosity η_{pl}) used in the numerical analysis are experimental values for high-flow mortar obtained in sphere drag tests as presented in an earlier report[4]. The materials used and their mix proportions are given in **Tables 1** and **2**, respectively. **Table 3** shows the yield value τ_y and plastic viscosity η_{pl} obtained by linear regression using with an equation by Ansely et al.[13], given here as Eq. (25), for pull-up rate v and drag force F in sphere drag tests.

$$F = 3\pi\eta_{pl}vD + \frac{7}{8}\pi^2D^2\tau_y \tag{25}$$

where, D = diameter of the steel sphere (31.75 mm).

Table 3 also gives the ratio of plastic viscosity η_{pl} to yield value τ_y, η_{pl}/τ_y, and the slump flow *Sfs* measured at the start of the sphere drag test (15 min after mixing) and the slump flow *Sfe* measured at the end of the sphere drag test.

The density (or mass per unit volume) of mortar is as calculated from the mix proportions given in **Table 2.** That is, the density is given as 2.187 × 10^{-3} g/mm^3 for M35%, Mc0.5%, and Mc0.25% with water/binder (W/B) ratios of 35% in each case, as 2.237 × 10^{-3} g/mm^3 for M30% with a water/binder (W/B) ratio of 30%, and as 2.140 × 10^{-3} g/mm^3 for M40% with a water/binder ratio of 40%.

Table 1 Materials used for high-flow mortar

Binder (B)	Ordinary Portland cement (OPC) Density: 3.16×10^{-3} g/mm^3 Blaine specific surface area: 3,270 cm^2/g
	Ground granulated blast-furnace slag (BFS) SO_3: 1.9% Density: 2.89×10^{-3} g/mm^3 Blaine specific surface area: 5,840 cm^2/g
Fine aggregate	Soma sand (S) No. 3: No. 4: No. 6 = 1:1:1 Density: 2.60×10^{-3} g/mm^3, F.M.: 2.46
Viscous agent	Cellulose ether base (c)
Super plasticizer	Polycarboxylic acid base (SP)

Table 2 Mix proportions of high-flow mortar

	No.	W/B (%)	S/B	Air (%)	Unit mass (kg/m^3) W	OPC	BFS	S	MC	SP
M30%	1	30	1.5	3.0	240	240	559	1198	-	5.19
	2									5.59
	3									5.99
	4									6.39
	5									6.95
	6									6.79
	7									7.19
	8									7.99
M35%	1	35			269	230	537	1151	-	3.22
	2									3.22
	3									3.84
	4									4.22
	5									4.60
	6									4.76
	7									5.14
M40%	1	40			295	221	517	1107	-	3.17
	2									3.47
	3									4.06
Mc0.5%	1	35			269	230	537	1151	1.345	6.14
	2									6.90
	3									7.67
	4									9.20
	5									9.20
	6									11.51
	7									15.34
Mc0.25%	1								0.6725	4.99
	2									5.37
	3									5.75
	4									6.14
	5									5.75
	6									6.90
	7									7.67

Table 3 Experimental results for high-flow mortar

	No.	Rheological coefficients τ_y (Pa)	η_{pl} (Pa·s)	η_{pl}/τ_y (s)	Slump flow Sfs (mm)	Sfe (mm)
M30%	1	121	60	0.5	493	484
	2	83	41	0.5	542	537
	3	45	37	0.8	599	604
	4	34	28	0.8	653	654
	5	19	23	1.2	732	728
	6	13	22	1.7	761	758
	7	10	21	2.1	793	783
	8	2.8	14	5.0	900	885
M35%	1	102	33	0.3	500	488
	2	106	18	0.2	512	503
	3	44	17	0.4	610	608
	4	32	15	0.5	656	643
	5	19	13	0.7	712	719
	6	15	11	0.7	735	748
	7	12	9.8	0.8	778	786
M40%	1	19	6.8	0.4	730	712
	2	17	6.8	0.4	726	719
	3	10	4.7	0.5	790	787
Mc0.5%	1	57	76	1.3	546	542
	2	80	74	0.9	551	548
	3	53	61	1.2	584	598
	4	35	53	1.5	624	644
	5	28	45	1.6	666	683
	6	24	42	1.8	701	703
	7	11	33	3.0	777	780
Mc0.25%	1	112	44	0.4	504	513
	2	72	43	0.6	562	553
	3	38	32	0.8	635	631
	4	30	29	1.0	670	655
	5	33	29	0.9	671	661
	6	14	24	1.7	749	755
	7	12	21	1.8	780	788

3.7 Choice of $\sqrt{I_{2_c}}$

When the square root of the second invariant of strain rate tensor $\sqrt{I_2}$ is no greater than the critical value $\sqrt{I_{2_c}}$, as already described, the relationship between $\sqrt{I_2}$ and $\sqrt{J'_2}$ is represented by the straight line given by Eq. (11). This line passes through the origin and has a slope of $2\left(\eta_{pl} + \tau_y / \left(2\sqrt{I_{2_c}}\right)\right)$. Therefore, it can be assumed that any deviation from the Bingham model can be reduced by choosing a small $\sqrt{I_{2_c}}$. The smaller the value of $\sqrt{I_{2_c}}$, the greater the viscosity η expressed by Eq. (15). As a result, the time step Δt required to meet the numerical stability condition expressed by Eq. (24) becomes shorter, thus increasing computation time.

In the sphere drag test conducted with a steel sphere of diameter D = 31.75 mm[4], it was confirmed that there is a linear relationship between pull-up rate v and drag force F in the pull-up range of 10 to 60 mm/s and also for pull-up rates up to 2 mm/s, depending on the yield value τ_y and the plastic viscosity η_{pl}. Assuming that samples near the sphere are subjected to simple shear in the sphere drag test, the shear strain rate e is given by the following equation, according to Eq. (3):

$$e = \sqrt{I_2} \qquad (26)$$

The sphere drag test also yields the following relationship between the shear strain rate e and the pull-up rate v[14]:

$$e = \frac{v}{2D} \qquad (27)$$

Using Eq. (27), the shear strain rate e is approximately 0.16 /s and 0.03 /s when the sphere pull-up rate is 10 and 2 mm/s, respectively. The above consideration suggests that $\sqrt{I_{2c}}$ should be set at a maximum of 0.16 /s, and that — depending on the yield value τ_y and plastic viscosity η_{pl} — it may be advisable to make it less than about 0.03 /s.

In this numerical analysis, therefore, $\sqrt{I_{2c}}$ is set at about 0.03 /s after taking into account its effect on computation time as well. This is coincidentally the same value as chosen by Yamada et al.[11].

4. Analytical Results and Discussion

4.1 Flow behavior

The flow of high-fluidity mortar as the slump cone is pulled up is successfully simulated by the numerical analysis. As an example of the analysis, the results for Mc0.5%-7 (yield value τ_y = 11 Pa; plastic viscosity η_{pl} = 33 Pa·s) are shown in **Fig. 3**. The positions of the marker particles are shown at intervals of about 0.28 s (10,000 steps) up to 1.69 s and about 1.13 s (40,000 steps) after 1.69 s. Of the 7,160 marker particles in total, every fourth one is plotted in **Fig. 3**.

As the vertical wall simulating the slump cone sidewall is pulled up to about 50 mm, it can be seen that the concrete begins to flow out through the gap below the sidewall and spread radially. Also clear from the results is that concrete adhering to the vertical sidewall flows directly down into the remainder of the sample with the elapse of time.

In this case, the sample is seen to slowly spread out radially after about 3 s.

4.2 Flow Radius and Flow Time

The speed of the sample's radial spread is obtained as the relationship between the r coordinate value (the flow radius) of edge marker particles and the time taken for the edge marker particles to reach that flow radius (referred to here as the flow time). **Figures 4** and **5** show this relationship between flow radius and flow time as derived from the numerical analysis in comparison with experimental values. The time plotted on the horizontal axis begins when the flow radius is 110 mm. The plot starts at this point in time so as to eliminate differences between the numerical analysis and the experiments in conditions immediately after slump cone pull-up begins. In the numerical analysis, an opening of 1 cell (5 mm) has already opened up below the vertical sidewall when computation begins ($t = \Delta t$). In the experiment, in contrast, measurements begin as soon as the slump cone starts to rise[4]. Setting the zero point on the time axis equivalent to a flow radius of 110 mm overcomes these discrepancies.

Figure 4 shows the analytical values and experimental values for Mc0.25%-6 (yield value τ_y = 14 Pa; plastic viscosity η_{pl} = 24 Pa·s). Also given are the analytical results for when the critical value of the square root of the second-order invariant of the strain rate tensor, $\sqrt{I_{2c}}$, is set at 0.16 /s and for when the slump cone is assumed to disappear as soon as the computation starts. Similarly, **Fig. 5** shows the analytical values and experimental values for Mc0.5%-6 (yield value τ_y = 24 Pa; plastic viscosity η_{pl} = 42 Pa·s).

A comparison of the numerical results with the experimental values confirms that the concrete flow is modeled with good accuracy, from the rapid spread in the initial stage, followed by a gradual fall in speed in the transition region, and finally to a stage of slow spread.

Figures 4 and **5** clearly show that, in cases where the slump cone disappears instantaneously or is assumed not to exist, the initial rate of radial spread is far greater in the analytical model than in experiments. On the other hand, when the effect of the slump cone sidewall is taken into account (with a slump cone pull-up rate of 40 mm/s), the analytical and experimental results agree well. This confirms the need to model the effect of the slump cone sidewall when the object of study is self-compacting concrete with a high deformation rate.

Comparing cases in which the critical value $\sqrt{I_{2c}}$ of the square root of the second invariant of strain rate tensor is set at 0.03 /s and at 0.16 /s, little difference is seen in the relationship between flow radius and flow time. However, in the final flow stage, when concrete spread is slow, the rate of spread is slightly faster in the case of

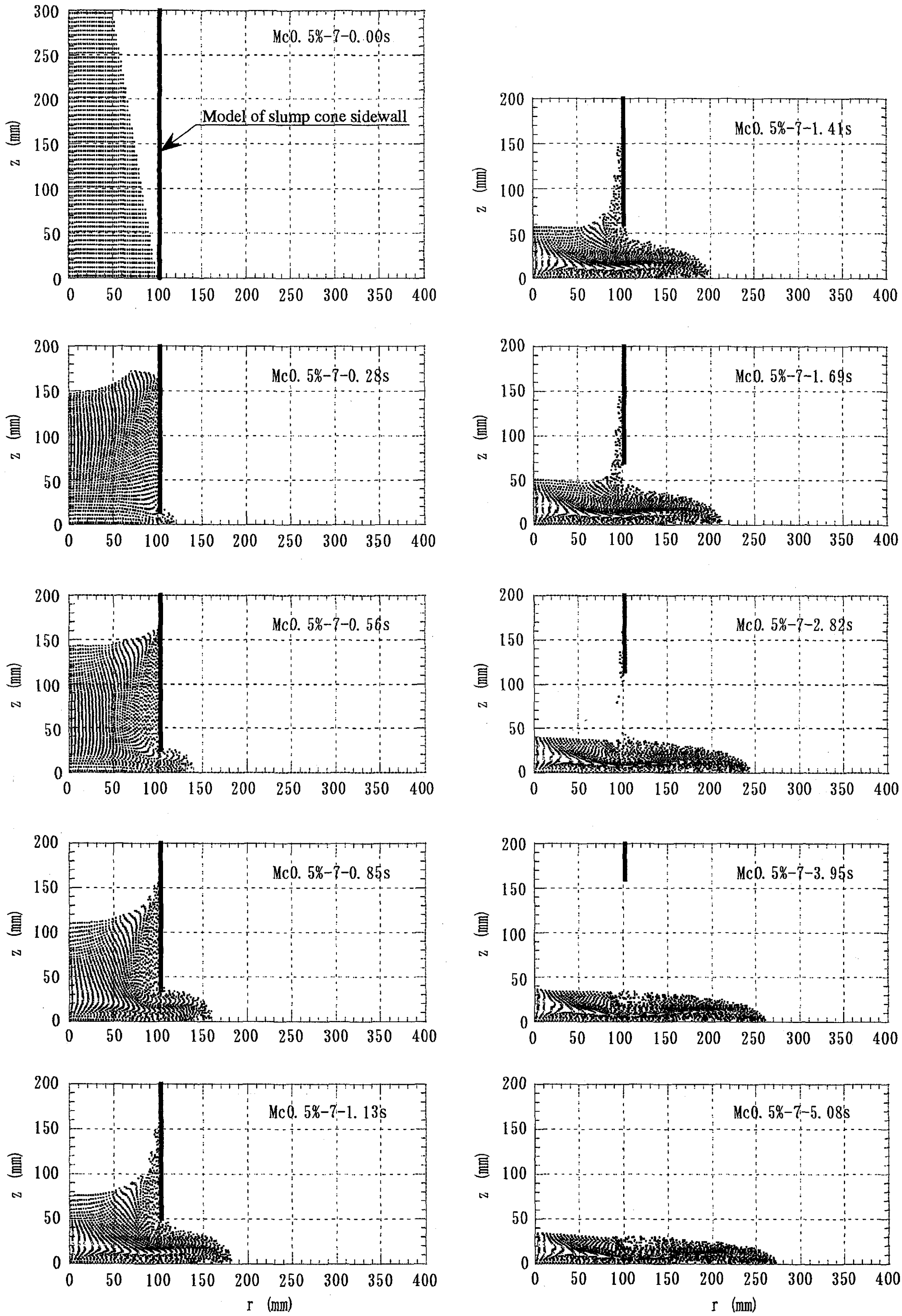

Fig. 3 Analytical results of Mc0.5%-7

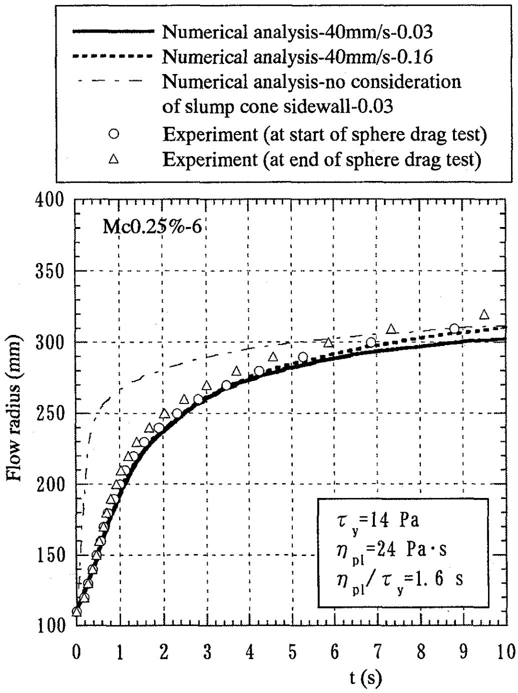

Fig. 4 Relationship between time and flow radius for Mc0.25%-6

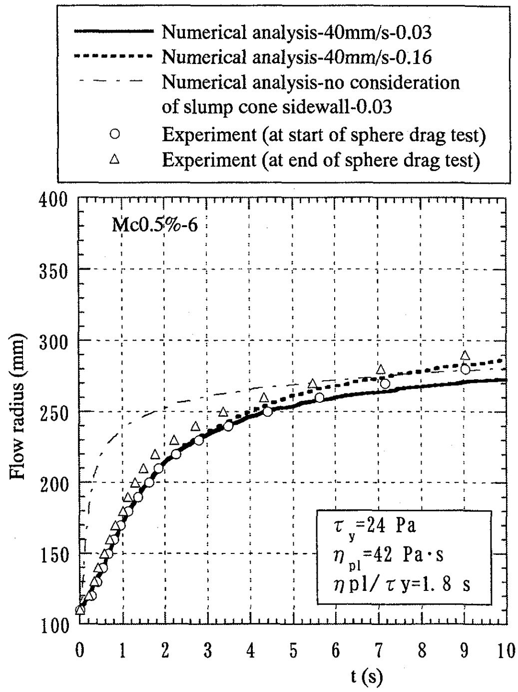

Fig. 5 Relationship between time and flow radius for Mc0.5%-6

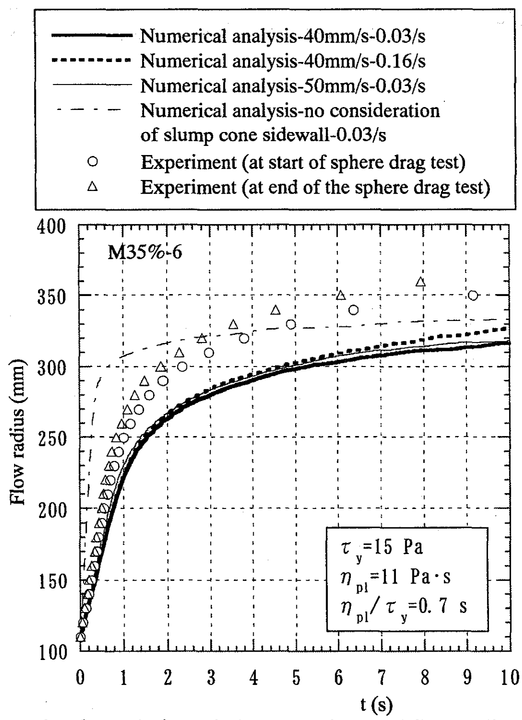

Fig. 6 Relationship between time and flow radius for M35%-6

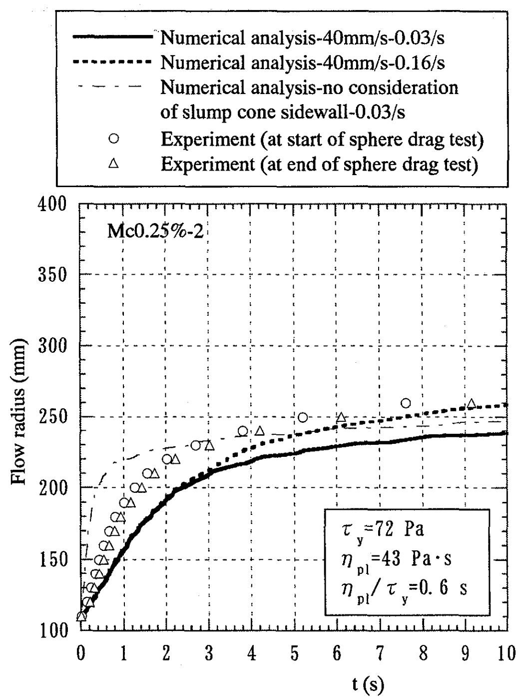

Fig. 7 Relationship between time and flow radius for Mc0.5%-2

$\sqrt{I_{2c}}$ = 0.16 /s than in the case of $\sqrt{I_{2c}}$ = 0.03 /s. This differential is larger for Mc0.5%-6 with a greater yield value.
The above discussion covers cases in which the analytical relationship between flow radius and flow time agrees well with experiment. Cases in which the agreement is poor are discussed below.
Figure 6 shows the relationship between flow radius and flow time for M35%-6 (yield value τ_y = 15 Pa; plastic viscosity η_{pl} = 11 Pa·s). The yield value τ_y of M35%-6 is almost the same as that of Mc0.25%-6 (as shown in **Fig. 4**), while its plastic viscosity η_{pl} is about a half. The analysis indicates a lower spread rate than seen in the experiments. The difference in flow time increases with increasing flow radius. The actual differences in the time taken to reach a flow radius of 200 mm is about 0.2 s. But the actual differences in the time taken to reach a flow radius of 250 mm are 0.5 s and 0.7 s, respectively, and the experimental values are 0.65 and 0.54 times the analytical values. As the flow radius increases, this differences increase further.
In the authors' experiment[4], the rate at which the slump cone was pulled up was sometimes influenced by the viscosity of the concrete. To look into the influence of this variable, analysis was also carried out for a slump cone pull-up rate of 50 mm/s. This difference in pull-up rate is found to have no appreciable effect on flow time.
Figure 7 shows the relationship between flow radius and flow time for Mc0.25%-2 (yield value τ_y = 72 Pa; plastic viscosity η_{pl} = 43 Pa·s). The yield value τ_y of Mc0.25%-2 is about three times greater than that of Mc0.5%-6, while its plastic viscosity η_{pl} is almost the same. The analytical values indicate lower spread speeds in the initial stage of flow than obtained in experiments, and the concrete takes nearly twice as long to reach a flow radius of 200 mm than in the experiment.
When the value of $\sqrt{I_{2c}}$ is set at 0.16 s, the concrete spread speed is greater in the last stage of flow than when $\sqrt{I_{2c}}$ is 0.03 s, but there is no difference in spread speed up to a flow radius of 200 mm.
The above demonstrates that numerical results may not agree with experimental values for certain combinations of yield value τ_y and plastic viscosity η_{pl}.

4.3 Analysis of Compatibility Conditions

As discussed above, the numerical results for flow time do not agree with experimental values in two situations: when the plastic viscosity η_{pl} is almost equal but the yield value τ_y is larger; and when the yield value τ_y is

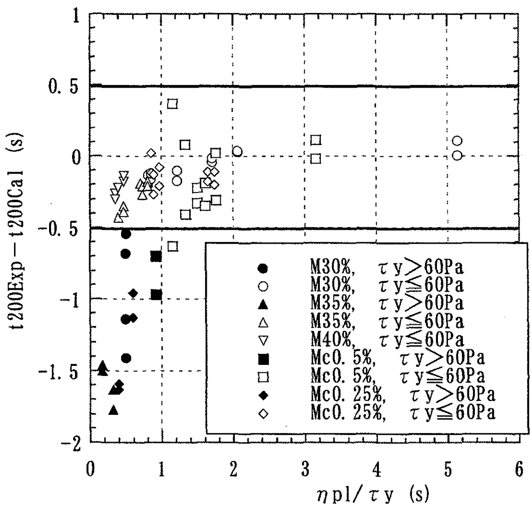

Fig. 8 Relationship between η_{pl}/τ_y and difference t200Exp − t200Cal

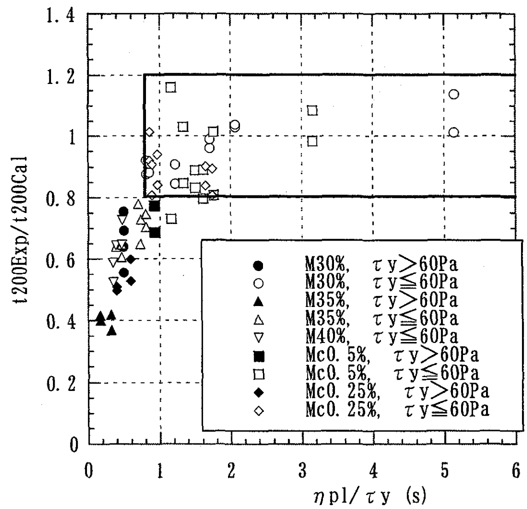

Fig. 9 Relationship between η_{pl}/τ_y and ratio t200Exp/t200Cal

almost equal but the plastic viscosity η_{pl} is smaller. The compatibility conditions of this numerical analysis are discussed here by focusing attention on the ratio of plastic viscosity η_{pl} to yield value τ_y, or the η_{pl}/τ_y ratio. The analytical values referred to below are the results of numerical analysis obtained under the conditions described in Section 3. In all cases, $\sqrt{I_{2c}}$ is 0.03/s and the slump cone pull-up rate is 40 mm/s. **Figure 8** shows the relationship between η_{pl}/τ_y ratio and the difference between experimental and analytical values of 200-mm flow time (t200Exp-t200Cal). When the yield value τ_y is 60 Pa or less, the difference between experimental and analytical values is ±0.5 s or less. **Figure 9** shows the relationship between the ratio t200Exp/t200Cal of the experimental value to the analytical value of the 200-mm flow times. When the η_{pl}/τ_y ratio is greater than 0.8 s, the t200Exp/t200Cal ratio falls within 1.0 ± 0.2. When the η_{pl}/τ_y ratio is less than 0.8 s, the experimental flow time is less than the analytical value, and the t200Exp/t200Cal ratio falls below 0.8. However, whether or not t200Exp/t200Cal falls below 0.8 is not related to the magnitude of the yield value τ_y. It should thus be recognized that when the viscosity is relatively low and the flow time is short, analysis does not always agree with experiment as determined by the t200Exp/t200Cal ratio. This is the case even if the t200Exp/t200Cal ratio is within ±0.5 s, as is the case with M35%-6 shown in **Fig. 6**.

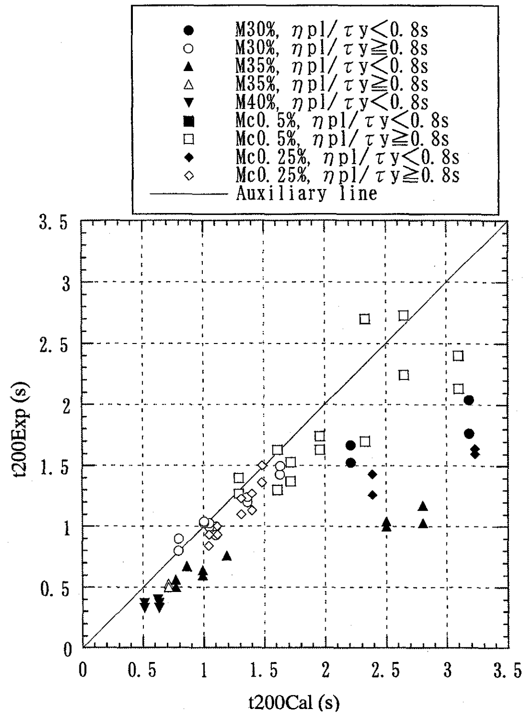

Fig. 10 Relationship between t200Cal and t200Exp

Figure 10 shows the same results as **Fig. 9** but redrawn as a relationship between t200Cal and t200Exp. When η_{pl}/τ_y > 0.8 s, as indicated by the open symbols, the analytical values agree closely with the experimental values.

When η_{pl}/τ_y < 0.8 s, shown by the solid symbols, the data can be divided into two groups. In one group,

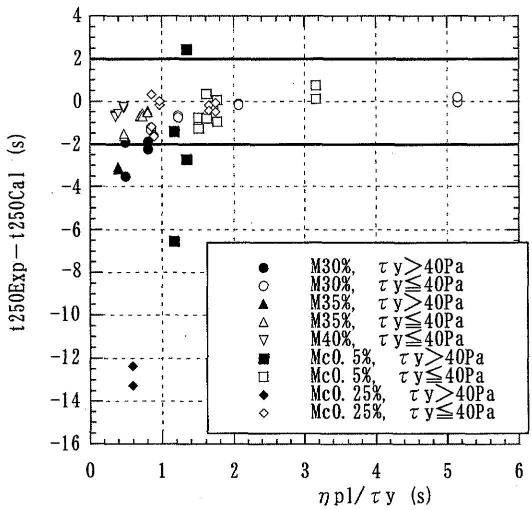

Fig. 11 Relationship between η_{pl}/τ_y and difference t250Exp−t250Cal

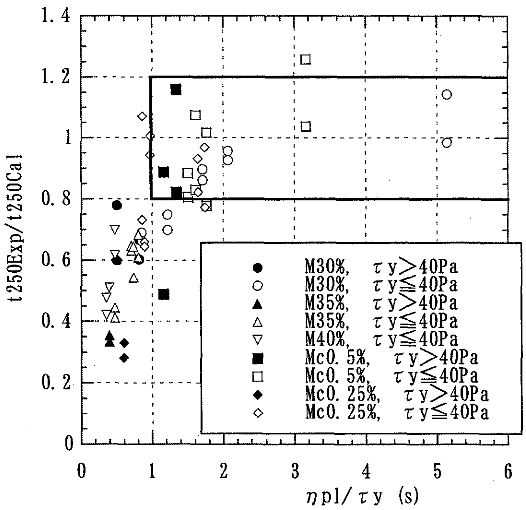

Fig. 12 Relationship between η_{pl}/τ_y and ratio t250Exp/t250Cal

the flow time is short and the difference between experimental values and analytical values is within ±0.5 s. In the other group, the flow time is long and the difference exceeds ±0.5 s.
As far as the time taken to reach the 250-mm flow radius is concerned, the relationship between η_{pl}/τ_y ratio and t250Exp-t250Cal is shown in **Fig. 11.** The relationship between the η_{pl}/τ_y ratio and the t250Exp/t250Cal ratio is shown in **Fig. 12.** The value of t250Exp-t250Cal difference is within ±2.0s when the yield value τ_y is 40 Pa or more. The t250Exp/t250Cal ratio increases toward 1 with increasing η_{pl}/τ_y ratio, as is the case with the 200-mm flow radius. The 250-mm flow time falls within 1.0 ± 0.2 s, except for some data when the η_{pl}/τ_y ratio is 1.0 s or more. From **Fig. 13,** it is confirmed that the analytical values agree well with the experimental values for η_{pl}/τ_y ratios of 1.0 s or more. The numerical analysis is thus confirmed to model the relationship between flow radius and flow time with quite accuracy (±20%) when the ratio of plastic viscosity to yield value, or the η_{pl}/τ_y ratio, is 1.0 s or more.

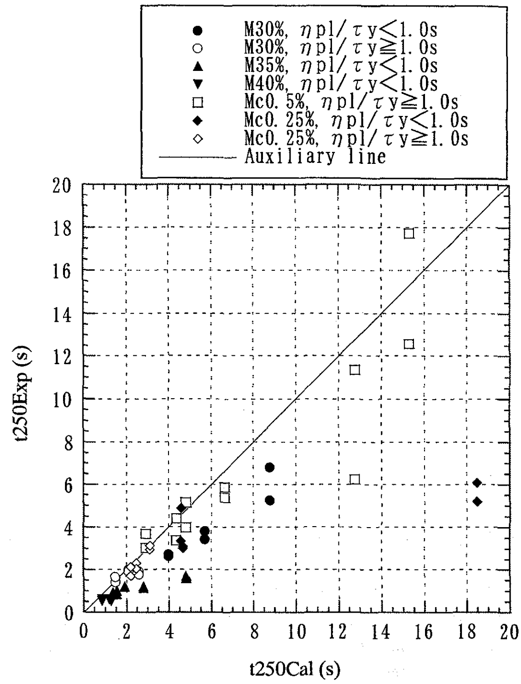

Fig. 13 Relationship between t250Cal and t250Exp

5. Relationship between rheological coefficients and flow time as determined by numerical analysis

The relationship between flow radius and flow time as determined by numerical analysis is confirmed to agree well with experiment for η_{pl}/τ_y ratios of 1.0 s or more. It follows then that the effects of plastic viscosity η_{pl} and yield value τ_y on flow time can be quantified numerically when the η_{pl}/τ_y ratio is 1.0 s or more.

Figure 14 shows the effects of yield value τ_y and plastic viscosity η_{pl} on flow time as determined by numerical analysis when the mass per unit volume V is 2.187×10^{-3} g/mm^3 (equivalent to that of mortar mixes M35%, Mc0.5%, and Mc0.25% with a water/binder (W/B) ratio of 35% as indicated in Table 2). The flow time is expressed as "0" when the flow radius reaches 110 mm.
The rheological coefficient plastic viscosity η_{pl} has a dominant effect on the 200-mm flow time t200Cal, while the yield value τ_y has no such appreciable effect. The 250-mm flow time t250Cal is found to be greatly affected by the yield value τ_y as well as the

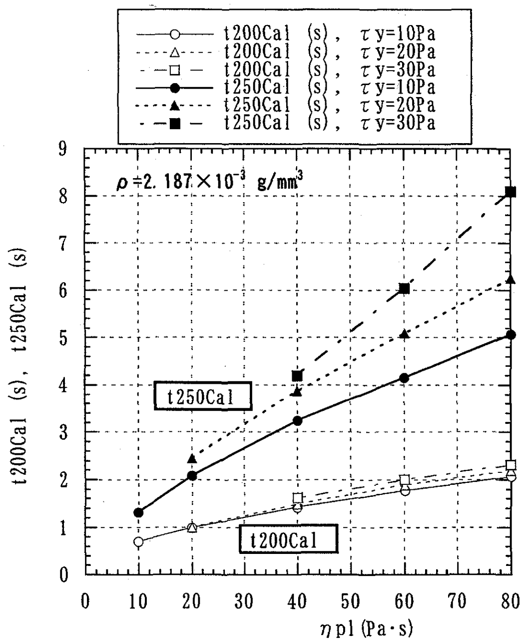

Fig. 14 Relationship between plastic viscosity η_{pl} and flow time obtained by numerical analysis

plastic viscosity η_{pl} .

This quantitatively demonstrates that the time taken to reach a given flow radius is influenced not only by the plastic viscosity η_{pl} , but also by the yield value τ_y . It is thus necessary to evaluate the yield value as well when using the time taken to reach a flow radius of 250 mm (or a flow diameter of 500 mm)[1] in the mix design or field quality control of self-compacting concrete.

6. Evaluation of Rheological Coefficients of Self-compacting Concrete by Slump Flow Test

When the ratio of plastic viscosity to yield value, η_{pl} / τ_y , of a self-compacting concrete that can be approximated by a Bingham fluid is 1.0 s or more, it has been demonstrated that numerical analysis is able to model the relationship between flow radius and flow time with high accuracy. Thus, if a self-compacting concrete containing coarse aggregate does in fact exhibit the flow behavior of a Bingham fluid, it can be considered practical to evaluate its rheological coefficients by numerical fluid analysis from the relationship between flow radius and flow time. This section describes an actual method for evaluating the rheological coefficients of self-compacting concrete from these slump measurements.

6.1 Test Description

Self-compacting concrete is generally more influenced by the unit water content than ordinary concretes[1]. The authors have attempted to quantitatively clarify, using theoretical equations[3] and numerical analysis, the variations in viscosity of self-compacting concrete with surface moisture of the aggregate.

6.2 Materials and Mix Proportions

The materials used in the tests are listed in **Table 4.** Ordinary Portland cement (OPC) and ground granulated blast furnace slag (BFS) were used as binders (B), and the slag replacement ratio (SR) was kept constant at 70%. Sand from Amaha, Chiba Prefecture, was used as the fine aggregate (S), and crushed hard sandstone 2005 from kuzuu, Tochigi Prefecture, was used as the coarse aggregate.

Two self-compacting concrete mixes were tested. One was the basic mix C32% set by referring to mix examples of powder-based self-compacting concrete[15], [16], [17], and the other was C29% with a surface moisture content of the fine aggregate 2% greater than in the basic C32% mix. **Table 5** shows these two self-compacting concrete mixes.

Mixing operations were performed in a dual mixer (with a capacity of 50 liters and a speed of 62 rpm) in a

Table 4 Materials used for self-compacting concrete

Binder (B)	Ordinary Portland cement (OPC) Density: 3.16×10^{-3} g/mm^3 Blaine specific surface area: 3,270 cm^2/g
	Ground granulated blast-furnace slag (BFS) SO_3: 2.5% Density: 2.89×10^{-3} g/mm^3 Blaine specific surface area: 6,120 cm^2/g
Fine aggregate(S)	Sand Density: $2.60\times$10- g/mm^3, Water absorption: 1.43 % Solid content: 66.5%, F.M.: 2.46
Coarse aggregate(G)	Crushed stone Density: 2.66×10^{-3} g/mm^3, Water absorption: 0.41 % Solid content: 60.5 %, F.M.: 6.75
Super plasticizer	Polycarboxylic acid base (SP)

thermostatic chamber. The mixer was charged with the binder, fine aggregate, and coarse aggregate in that order and dry mixed for 15 s. After adding water and superplasticizer, the ingredients were mixed for 3 minutes.

6.3 Test Methods

After each sample had stabilized for 15 minutes after mixing[3], it was removed from the mixer and subjected to a slump flow test, a V-shaped funnel test, a U-shaped funnel gap penetration test, and an air content test according to the recommendations of the Japan Society of Civil Engineers[1]. In the slump flow test, the time taken for the sample edge to reach marks placed at intervals of 10 mm (flow time) was recorded by video photography[3]. After measuring the slump flow, the height distribution of the sample was measured in the radial direction at intervals of 20 mm from the sample center. The V-shaped funnel test was conducted using two V75 funnels each with an outlet of 75 mm. The U-shaped funnels had a type-R2 flow obstruction. The maximum fill height $B_{h\text{-}max}$ of the U-shaped funnels was 367 mm.

Table 5 Mix proportions of self-compacting concrete

		W/B	s/a	Air	Unit mass (kg/m^3)					
	No.	(%)	(%)	(%)	W	OPC	BFS	S	G	SP
	1									10.94
C32%	2									10.99
	3									10.99
	4	32	50.9		175	164	383	801	798	11.05
	5									11.05
	6									11.05
	7									11.21
	8									11.21
	9			3.0						12.03
	1									13.55
C29%	2									13.55
	3									13.66
	4	29	51.3		161	166	387	824	806	13.66
	5									13.66
	6									13.83
	7									13.83
	8									13.83

6.4 Test Results

a) List of Test Results

Table 6 Test results (1) for self-compacting concrete

		Slump flow	Air	Flow time (s)					V_{75} funnel flow time		U-shaped funnel filling height (mm)
	No.	*Sf* (mm)	(%)	110mm flow time (s)	200mm flow time (s)	250mm flow time (s)	t200Exp (s)	t250Exp (s)	First time (s)	Second time (s)	
	1	560	2.8	1.37	3.13	7.00	1.76	5.63	8.9	10.2	311
C32%	2	605	4.9	0.40	2.07	4.50	1.67	4.10	9.7	9.3	337
	3	605	3.5	0.87	2.60	4.60	1.73	3.73	9.9	9.2	340
	4	633	4.2	1.10	2.73	5.10	1.63	4.00	8.9	8.7	342
	5	640	3.4	1.00	2.57	4.23	1.57	3.23	8.9	8.2	361
	6	650	3.3	0.87	2.30	3.97	1.43	3.10	7.8	8.9	341
	7	680	4.2	0.87	2.43	4.20	1.56	3.33	8.0	8.2	362
	8	683	3.2	0.43	1.87	3.67	1.44	3.24	8.9	8.2	362
	9	730	3.5	0.47	1.83	3.20	1.36	2.73	6.7	7.3	360
	1	620	3.4	1.30	3.67	7.10	2.37	5.80	17.3	17.0	322
C29%	2	630	2.8	1.53	3.67	6.97	2.14	5.44	17.2	18.5	345
	3	648	3.7	1.10	3.63	6.93	2.53	5.83	18.1	16.1	347
	4	650	2.9	1.43	3.63	6.70	2.20	5.27	15.8	15.5	348
	5	650	2.7	1.27	3.63	6.70	2.36	5.43	13.8	13.2	358
	6	670	3.0	1.60	3.97	7.27	2.37	5.67	14.8	16.0	357
	7	675	3.0	1.37	3.70	6.97	2.33	5.60	16.3	17.3	360
	8	683	2.7	0.97	3.23	5.70	2.26	4.73	14.4	15.5	360

The measurements of slump flow, air content, flow time, V75 funnel flow time, and U-shaped funnel (R2) fill height are given in **Table 6**. The flow time values consist of the time to reach the flow radii of 110 mm, 200 mm, and 250 mm. The 200-mm flow time t200Exp and the 250-mm flow time t250Exp, obtained by subtracting the 110-mm flow time, are also shown.

b) Flow Time

Figure 15 shows the time taken to reach each flow radius (as measured at 10-mm intervals) for C32% (C32%-5 and C32%-6) and C29% (C29%-3 and C29%-5), which have almost equivalent slump flows. It is recognized that, although the slump flows are almost equivalent, the time taken to reach the two flow radii clearly differs between C32% and C29%. **Figure 16** shows the relationship between slump flow *Sf* and the 200-mm flow time (t200Exp) and the 250-mm flow time (t250Exp). When C32% and C29% both are constant in mix proportions except for the superplasticizer in the test ranges, the 200-mm flow time, t200Exp, is not appreciably influenced by the variation of the slump flow.

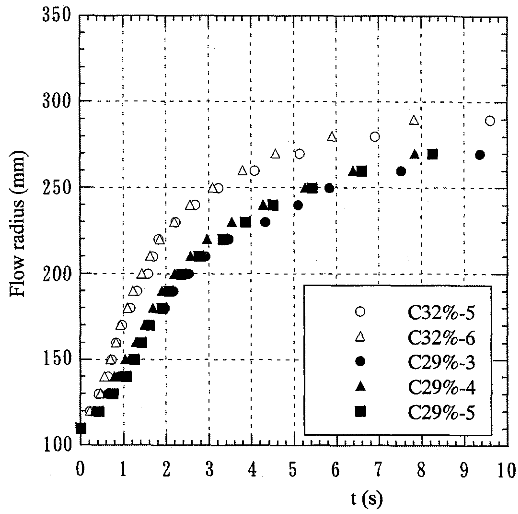

Fig. 15 Relationship between time and flow radius (C32%-5, C32%-6, C29%-3, C29%-4, C29%-5)

c) V-shaped Funnel Flow Time

Figure 17 shows the relationship between slump flow Sf and V-shaped funnel flow time. A clear difference in V-shaped funnel flow time is recognized between C32% and C29%. The V-shaped funnel flow time varies somewhat for C29%, but has a larger range of about 7 to 10 s for C32%. It is thus confirmed that the V-shaped funnel flow time is not appreciably influenced by the variation in slump flow, as noted for t200Exp. It is presumed that the V-shaped funnel test evaluates the flow characteristics of concrete in the region where the strain rate is relatively high and exhibits a tendency similar to that of the t200Exp value.

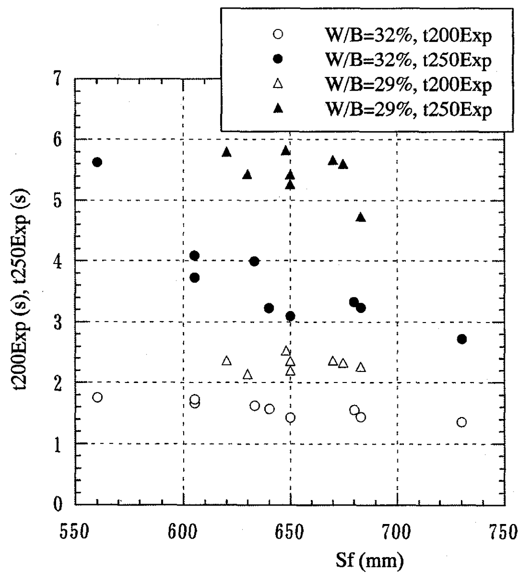

Fig. 16 Relationship between slump flow and t200Exp and t250Exp

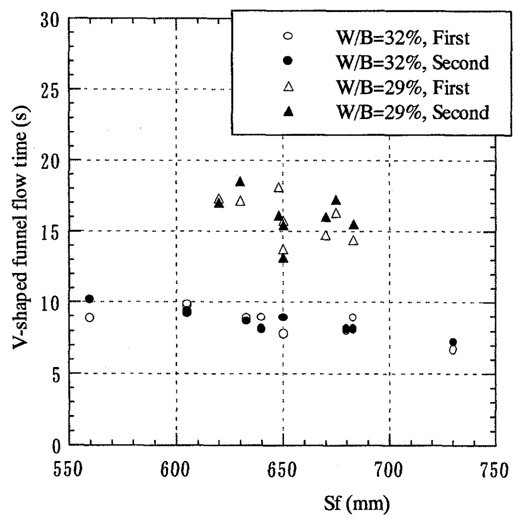

Fig. 17 Relationship between slump flow and V-shaped funnel flow time

d) U-shaped Funnel Filling Height

Figure 18 shows the relationship between slump flow Sf and U-shaped funnel fill height. The U-shaped funnel fill height is 300 mm or more, irrespective of the slump flow. Both C32% and C29% are judged to have good gap penetration characteristics in the test ranges studied.

e) Slump Cone Pull-up Rate

Figure 19 shows the relationship between slump flow Sf and slump cone pull-up rate measured from the recorded video. Despite some variability, the slump cone pull-up rate for self-compacting concrete ranges from about 40 to 60 mm/s as reported for high-flow mortar[4].

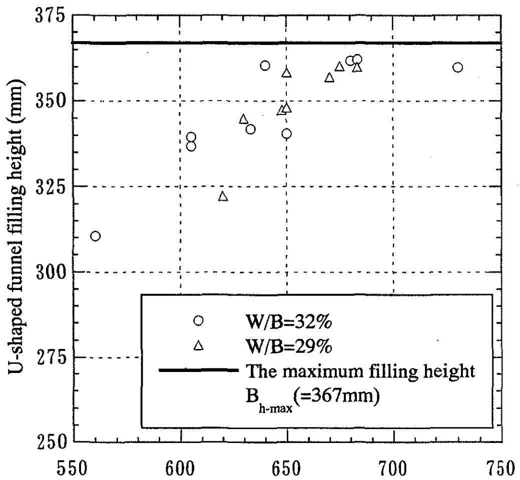

Fig. 18 Relationship between slump flow and U-shaped funnel filling height

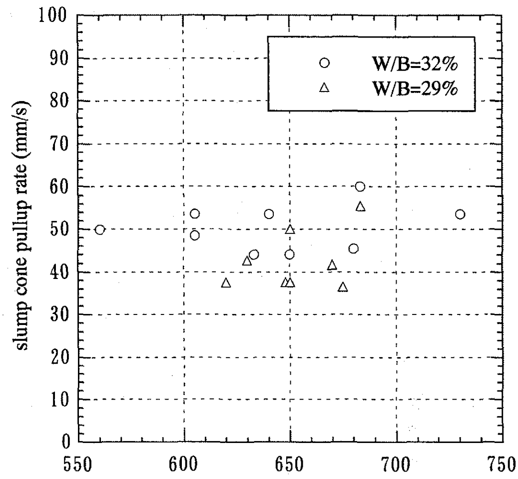

Fig. 19 Relationship between slump flow and slump cone pull-up rate

6.5 Evaluation of Yield Value

The yield value τ_{yF} is obtained by substituting slump flow Sf and sample volume V into Eq. (28), a theoretical equation[3] expressing the relationship between yield value and slump flow in slump flow tests.

$$\tau_{yF} = \frac{15^2 \rho g V^2}{4\pi^2 Sf^5} \qquad (28)$$

where, τ_{yF} is the yield value (Pa) obtained from the slump flow; Sf is the slump flow (mm); ρ is density (mass per unit volume) (g/mm^3); g is the acceleration due to gravity (mm/s^2); and V is the sample volume (mm^3).

The yield value τ_{yH} is obtained by performing regression analysis with L and τ_{yH} as fit parameters on the height distribution (r, z) measured at intervals of 20 mm in the radial direction from the center of the test sample. This is done using Eq. (29), a theoretical equation[3] expressing the sample height distribution.

$$\frac{z^2}{2} = (L - r)\frac{\tau_{yH}}{\rho g} \qquad (29)$$

where, τ_{yH} is the yield value obtained from the height distribution of the test sample (Pa); and L is the distance from the center to the edge of the sample (mm).

The height distribution of the sample and a regression

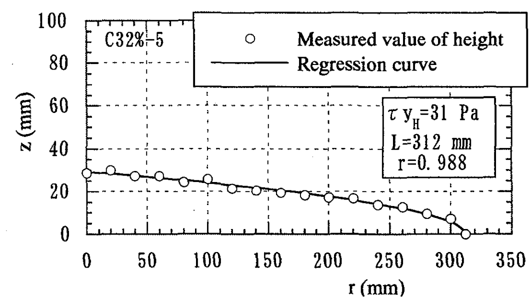

Fig. 20 Regression curve of height distribution

Table 7 Test results (2) for self-compacting concrete

	No.	Slump flow Sf (mm)	Volume of specimen V ($\times 10^6 mm^3$)	Normalized slump flow Sf_N (mm)	Yield value with Eq.(28) τ_{yF} (Pa)	Yield value with Eq.(29) τ_{yH} (Pa)	Correlation coefficient R
C32%	1	560	5.316	568	67	68	0.982
	2	605	5.335	612	46	46	0.987
	3	605	5.330	613	46	43	0.939
	4	633	5.370	638	37	45	0.946
	5	640	5.374	646	35	31	0.988
	6	650	5.373	656	32	34	0.980
	7	680	5.381	686	26	24	0.975
	8	683	5.341	690	25	22	0.982
	9	730	5.376	736	18	18	0.984
C29%	1	620	5.353	627	41	37	0.966
	2	630	5.334	638	38	34	0.966
	3	648	5.329	656	33	31	0.940
	4	650	5.328	658	32	33	0.922
	5	650	5.337	658	32	28	0.988
	6	670	5.334	678	28	26	0.979
	7	675	5.348	683	27	25	0.983
	8	683	5.339	691	25	24	0.938

curve obtained from the height distribution measurements are shown in **Fig. 20**.
Table 7 lists the yield value τ_{yF} obtained from the slump flow and the yield value τ_{yH} obtained from the sample height distribution. **Figure 21** shows the relationship between τ_{yF} and τ_{yH}. For the C29% mix, τ_{yF} tends to assume a somewhat larger value than τ_{yH}, but the two values agree closely with each other.

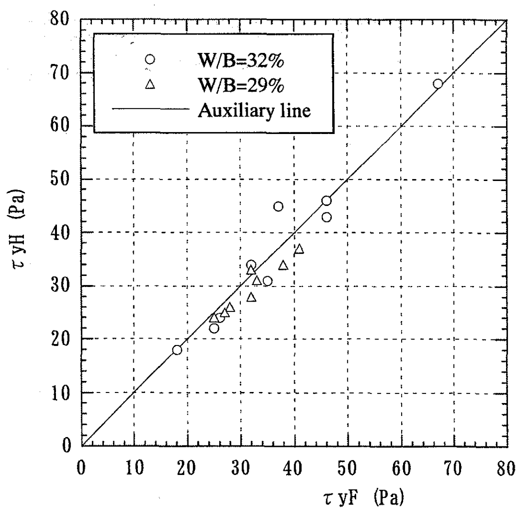

Fig. 21 Relationship between τ_{yF} and τ_{yH}

6.6 Evaluation of Plastic Viscosity by Numerical Analysis

The authors have attempted to quantitatively indicate through numerical analysis the difference in plastic viscosity of the basic C32% self-compacting concrete mix and the C29% mix with a fine aggregate surface moisture content set 2% higher than that of the basic C32% mix.

a) Analytical Premises

The numerical analysis was applied to mixes C32%-5, C32%-6, C29%-3, C29%-4, and C29%-5 with almost equivalent slump flow values of 640 to 650 mm, as shown in **Fig. 15**.
The mass per unit volume calculated from the mix proportions in **Table 5** is 2.321×10^{-3} g/mm^3 for the C32% mixes and 2.344×10^{-3} g/mm^3 for the C29% mixes. Since the mass per unit volume of C32% differs by a mere 1% or so from that of C29%, the value used in the numerical analysis is set at 2.321×10^{-3} g/mm^3.

As shown in **Table 7**, the yield value τ_{yF} calculated using Eq. (26) from the slump flow is 32 to 35 Pa for all mixes, and the yield value τ_{yH} calculated using Eq. (27) from the slump flow test sample height distribution ranges from 28 to 34 Pa for these mixes. The yield value used in the numerical analysis is thus set at a constant value of 30 Pa.
The measured slump cone pull-up rate is 54 mm/s for C32%-5, 44 m/s for C32%-6, 38 mm/s for C29%-3, 38 mm/s for C29%-4, and 50 mm/s for C29%-5.
Given this range, two values of slump cone pull-up rate v are used in the analysis: 40 and 50 mm/s. The other analytical conditions are as described in Section 3.

b) Analytical Results

Figure 22 shows the relationship between flow radius and flow time for one analytical case in which the plastic viscosity η_{pl} is 30 Pa·s and for another in which the η_{pl} is 80 Pa·s. The experimental values are also shown. As far as the relationship between flow radius and flow time is concerned, the experimental values tend to indicate a faster spread in the region where the flow radius is 250 mm or more, as observed for some test results of high-flow mortar. In the region up to a flow radius of 250 mm, the analytical results agree well with the experimental values. The plastic viscosity can thus be quantified as about 30 Pa·s for C32%-5 and C32%-6, and about 80 Pa·s for C29%-3, C29%-4, and C29%-5.
In these analytical cases, the relationship between flow radius and flow time (the time taken to reach a particular flow radius) in the slump flow test and in the numerical analysis indicates that, when the surface moisture content of the fine aggregate is set 2% higher than actually measured, the plastic viscosity increases by a factor of about 2.7.

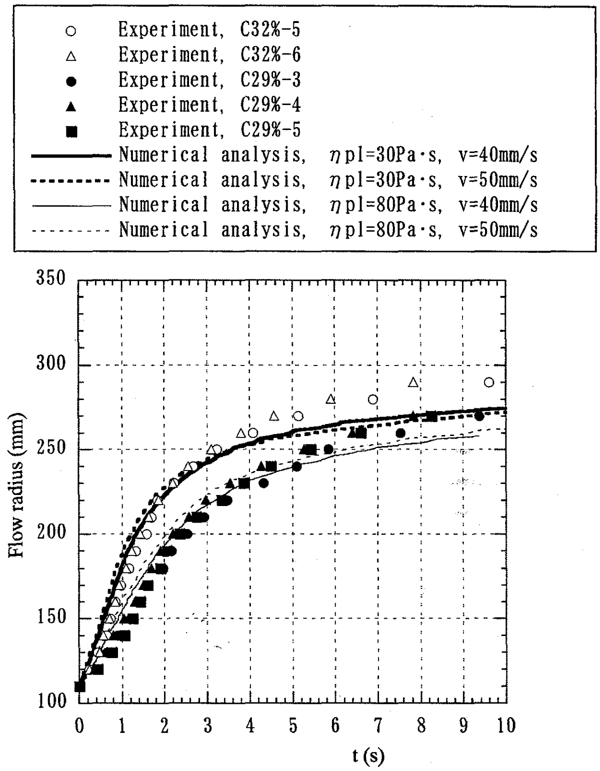

Fig. 22 Relationship between time and flow radius

7. Conclusions

This study has demonstrated the validity of a numerical model of the flow behavior of self-compacting concrete in the slump flow test and clarified its limitations through a comparison with experiments involving high-flow mortar. Further, the effects of the rheological coefficients (yield value and plastic viscosity) on the time to reach specific flow radii (the flow time) has been evaluated by numerical analysis in comparison with the effects of the rheological coefficients of high-flow mortar in slump flow tests.
The results of the study may be summarized as follows:
(1) When numerically analyzing self-compacting concrete with a high rate of deformation, it is necessary to model the effect of the slump cone sidewall as the slump cone is being pulled up.
(2) When the ratio of plastic viscosity to yield value, η_{pl}/τ_y, is 1.0 s or more, numerical analysis is able to model the relationship between flow radius and flow time of high-flow mortar with a quite accuracy of ±20%. When the η_{pl}/τ_y ratio is less than 1.0 s, the analytical values diverge from the experimental values. In this situation, it is likely that there is a discrepancy between the numerical analysis conditions and the actual flow and deformation behavior of high-flow mortar. It appears necessary to discuss the factors influencing separately for the regions of where the yield value τ_y is large and where it is small.

(3) As a rheological coefficient, the plastic viscosity has a dominant effect on the time taken to reach a flow radius of 200 mm. The time required to reach a flow radius of 250 mm is greatly affected by both plastic viscosity and also yield value.
(4) If self-compacting concrete contains a coarse aggregate and exhibits the flow behavior of a Bingham fluid, its rheological coefficients can be evaluated by numerical fluid analysis.

References

[1] JSCE: Recommendations for Construction Practice of Self-Compacting Concrete, July 1998.
[2] JASS: Recommendations for Mix Design and Construction Practice of High Fluidity Concrete, January 1997.
[3] Kokado, T., Hosoda, T., Miyagawa, T., and Fujii, M.: Study on a Method of Obtaining Yield Values of Fresh Concrete from Slump Flow Test (Translation from Proceedings of JSCE, No. 548/V-37, November 1977), *Concrete Library of JSCE*, No. 32, December 1998.
[4] Kokado, T. and Miyagawa, T.: Study on a Method of Obtaining Rheological Coefficients of Self-Compacting Concrete from Slump Flow Test, *Proc. of JSCE*, No. 634/V-45, pp. 113-129, November 1999.
[5] Fung, Y.C.: A First Course in Continuum Mechanics, *Prentice-Hall*, pp.202-203, 1994.
[6] Hatta, N.: Calculation of Flow, *Morikita Shuppan*, pp. 82-117, January 1994.
[7] Harlow, F.H. and Welch, J.E.: Numerical Calculation of Time-Dependent Viscous Incompressible Flow of Fluid with Free Surface, *Physics of Fluids*, Vol. 8, No. 12, 1965.
[8] Mori, H. and Tanigawa, Y.: Simulation of Flow Behavior of Fresh Concrete by Visco-plastic Element Analysis, *Transactions of AIJ*, No. 374, pp. 1-9, April 1984.
[9] Nabeta, K., Machida, A., Iwashita, K., and Sasaki, T.: Flow Simulation of Fresh Concrete by Distinct Element Method, *Proceedings of JCI*, Vol. 16, No. 1, pp. 479-484, 1994.
[10] Ishiguro, K. and Tomiya, J.: Flow Simulation of Fresh Concrete, *Proc. of the 50th Annual Conference of JSCE*, pp. 1028-1029, 1995.
[11] Yamada, Y., Ohshiro, T., and Masuda, Y.: Application of MAC Method to Flow Analysis of Fresh Concrete, *Proc. of JCI*, Vol. 20, No. 1, pp. 131-136, 1998.
[12] Roache, P.J.: Computational Fluid Dynamics, *Hermosa Publishers*, 1976.
[13] Ansley, R.W. and Smith, T.N.: Motion of Spherical Particles in a Bingham Plastic, *AIChE Journal*, Vol. 13, No. 6, pp. 1193-1196, November 1967.
[14] JSCE: Guidelines for Measuring Properties of Fresh Concrete, *Proc. of Symposium on Properties of Fresh Concrete and Their Application in Concreting Practice*, pp. 190-192, March 1986.
[15] Kokado, T. and Miyake, M.: A Field Test on Self-Compacting Concrete with Ground Granulated Blast-Furnace Slag, *Proc. of JCI*, Vol. 13, No. 1, pp. 875-880, 1991.
[16] Yokoyama, M., Egawa, S., Tanaka, M., Matsuoka, A., and Kokado, T.: Study on Applicability of Self-Compacting Concrete to Steel-Concrete Sandwich Structures, *Proc. of 48th Annual Conference of JSCE*, Part VI, pp. 248-249, 1993.
[17] Kokado, T., Suzuki, Y., Wako, T., and Sato, S.: Characteristics of Powder-Based Self-Compacting Concrete for Filling in Full Sandwich Structure of Submersed Tunnel, *Proc. of JCI*, Vol. 17, No. 1, pp. 191-196, 1995.